

## Article

# Modification of LaB<sub>6</sub> with ZrO<sub>2</sub>-Al<sub>2</sub>O<sub>3</sub>-TiO<sub>2</sub> for Improvement of Density and Mechanical and Electrical Properties

Sen Yang, Ruiqing Ba, Jingnan Hong, Jing Li, Jingdong Guo, Xinghui He, Hongwei Zhang, Naihe Yi and Weibing Ma \*

Key Laboratory of Advanced Ceramics and Machining Technology of Ministry of Education, School of Materials Science and Engineering, Tianjin University, Tianjin 300072, China; 2021208040@tju.edu.cn (S.Y.)

\* Correspondence: tju11305@126.com

**Abstract:** Pure lanthanum hexaboride (LaB<sub>6</sub>) ceramics were prepared using powders of different grain sizes. The ceramics could reach a relative density of 98.2% at high temperatures and pressures, but had a low flexural strength (136.9 MPa). LaB<sub>6</sub> ceramics were synthesized using ZrO<sub>2</sub>-Al<sub>2</sub>O<sub>3</sub>-TiO<sub>2</sub> (ZAT) as sintering additives. The ceramics demonstrate high density and excellent mechanical properties. The hot pressure sintering (HPS) method was utilized in the synthesis of the ceramics. Investigations were conducted on the effects of ZAT content, as well as the effects of the sintering temperature and pressure on the sintering behavior, microstructure, and mechanical and electrical properties of LaB<sub>6</sub> ceramics. LaB<sub>6</sub> ceramics fabricated with a ZAT addition of 6 wt.%, at a sintering temperature of 1700 °C, and under a pressure of 50 MPa, exhibited superior sintering and electrical properties, including a relative density of 97%, a conductivity of 7.2 MS/m, a flexural strength of 281.5 MPa, and a Vickers hardness of 21.2 GPa. The LaB<sub>6</sub> ceramics synthesized in this research exhibit promising potential as electron-emitting cathodes for field emission applications.

**Keywords:** ZAT; LaB<sub>6</sub>; electrical conductivity; mechanical property; hot pressing



**Citation:** Yang, S.; Ba, R.; Hong, J.; Li, J.; Guo, J.; He, X.; Zhang, H.; Yi, N.; Ma, W. Modification of LaB<sub>6</sub> with ZrO<sub>2</sub>-Al<sub>2</sub>O<sub>3</sub>-TiO<sub>2</sub> for Improvement of Density and Mechanical and Electrical Properties. *Crystals* **2024**, *14*, 452. <https://doi.org/10.3390/cryst14050452>

Academic Editor: Maria Gazda

Received: 15 April 2024

Revised: 29 April 2024

Accepted: 7 May 2024

Published: 9 May 2024



**Copyright:** © 2024 by the authors. Licensee MDPI, Basel, Switzerland. This article is an open access article distributed under the terms and conditions of the Creative Commons Attribution (CC BY) license (<https://creativecommons.org/licenses/by/4.0/>).

## 1. Introduction

In 1951, Lafferty identified that LaB<sub>6</sub> possesses excellent hot electron emission properties [1]. Since then, rare earth hexaborides have attracted significant attention from researchers [2,3]. LaB<sub>6</sub> is regarded as an ideal material for electron-emitting cathodes owing to its low work function, high mechanical strength, and chemical stability [4–7].

The magnitude of the work function is primarily dependent on the electronic structure of the atoms in the solid's near-surface layer [8]. The work function varies naturally with the phase of matter. Even within the same phase, the density of atoms and the density of the 'electron cloud' may vary across different crystalline surfaces. The polar moments of the dipole layers as well as the work function vary. Furthermore, foreign adsorbed atoms exert a significant effect on the work function. Research has shown that the low work function of LaB<sub>6</sub> results from the formation of a La-B dipole layer on the surface [9].

Compared to the LaB<sub>6</sub> single crystal, polycrystalline blocks (LaB<sub>6</sub> ceramics) offer more straightforward preparation methods and larger sizes, making them suitable for a wide range of applications [10,11]. However, their poorer mechanical properties (Vickers hardness: 5~15 GPa; flexural strength: 80~150 MPa) and lower conductivity (3.3~10 MS/m) as well as high work function (>2.8 eV) limit their use. To overcome these limitations, current research on LaB<sub>6</sub> polycrystalline materials mainly focuses on three aspects: enhancing densification, achieving fine crystallization [12], and developing multiphase compositions [5,13–15].

The mechanical properties and electron emission properties of LaB<sub>6</sub> ceramics deteriorate as densities decrease. Common strategies for promoting the high densification of LaB<sub>6</sub> ceramics include employing high-temperature and high-pressure process conditions, along with finer nanopowders.

Zhou et al. [12] found that the mechanical properties and the thermoelectric emission properties of LaB<sub>6</sub> polycrystalline material could match those of LaB<sub>6</sub> single-crystal material when the grain size was reduced to the nanoscale. The nanocrystal LaB<sub>6</sub> hardness was 22.3 GPa, the flexural strength was 271.2 MPa, and the maximum emission current density was 56.81 A·cm<sup>-2</sup> at a cathode temperature of 1600 °C. Research into high densification and fine crystallization includes the use of nanomaterials and spark plasma sintering (SPS) for preparing high-density ceramics to investigate their thermoelectric emission properties. However, SPS produces samples with limited size, presenting complexities and high operational costs that preclude industrial production. In contrast, the HPS method enables the industrial production of larger samples. Research on multiphase composition predominantly focuses on adding rare earth elements to synthesize binary or polyhexaborides, as well as preparing high-entropy hexaborides to explore their functional and electron emission properties. Furthermore, researchers have explored the addition of ZrB<sub>2</sub> and other borides to enhance the physical properties of LaB<sub>6</sub>, such as strength and toughness [16,17]. However, these raw materials are not only expensive and challenging to prepare, but the resulting performance enhancement is also limited.

Compared to diborides like ZrB<sub>2</sub>, oxides typically exhibit lower melting points, which leads to the formation of liquid phases or other reactions that facilitate sintering. For example, Si<sub>3</sub>N<sub>4</sub> ceramic sintering frequently utilizes Y<sub>2</sub>O<sub>3</sub> and Yb<sub>2</sub>O<sub>3</sub> as sintering additives, while also occasionally including Al<sub>2</sub>O<sub>3</sub> and MgO [18–20]. SiC presents challenges in sintering for densification due to its high covalent bond ratio. Typically, sintering additives comprise oxides such as Al<sub>2</sub>O<sub>3</sub>, Y<sub>2</sub>O<sub>3</sub>, CeO<sub>2</sub>, and Er<sub>2</sub>O<sub>3</sub> [21–23]. While promoting sintering, the addition of oxides also enhances the mechanical strength of the material.

TiB<sub>2</sub> and ZrB<sub>2</sub> are commonly used for LaB<sub>6</sub> modification [16,17]. The corresponding oxides TiO<sub>2</sub> and ZrO<sub>2</sub> were selected, followed by the addition of Al<sub>2</sub>O<sub>3</sub> as a sintering aid, named as ZAT. By utilizing the properties of polyoxides with a low eutectic point and applying additional pressure during the sintering process to increase mobility, it is possible to eliminate pores and enhance the material's density. In our application scenario, cold-field emission is involved, indicating that low temperatures prevail and the inclusion of oxides does not result in the poisoning of the LaB<sub>6</sub> cathode or the degradation of mechanical properties to the point of being unusable. Polycrystalline LaB<sub>6</sub> contains a small amount of oxide as a second phase, which is located at the grain boundaries. This second phase may absorb energy during fracture, thereby increasing the flexural strength of LaB<sub>6</sub> ceramics. Given that oxides diminish the thermal conductivity of Si<sub>3</sub>N<sub>4</sub>, it warrants investigation into whether this impacts the exceptional electrical conductivity of LaB<sub>6</sub> itself. This study examines the relative density, electrical conductivity, and flexural strength of LaB<sub>6</sub> ceramics.

## 2. Materials and Methods

### 2.1. Materials

LaB<sub>6</sub> powder (with an average particle size of 20 μm and 10 μm) was provided by Shanghai Yao Tian Nano Material Co., Ltd. (99.5%, Shanghai, China); ZrO<sub>2</sub> was purchased from Kermel (99.0%, Tianjin, China); Al<sub>2</sub>O<sub>3</sub> was purchased from Heowns (99.0%, Tianjin, China); and TiO<sub>2</sub> was purchased from Aladdin (99.0%, Shanghai, China).

### 2.2. Preparation

In the experiment, ZrO<sub>2</sub>, Al<sub>2</sub>O<sub>3</sub>, and TiO<sub>2</sub> were combined in a mass ratio of 46%: 34%: 20%, and then thoroughly mixed with deionized water using a planetary ball mill at 300 r/min for 6 h. Following the ball milling process, the mixed powder was dried in an oven at 120 °C before being passed through a 100-mesh sieve. The powder obtained was designated ZAT.

LaB<sub>6</sub> powders with varying amounts of ZAT (3–8 wt.%) were comprehensively mixed with deionized water using a planetary ball mill at 300 r/min for 6 h. Following the ball milling, the mixed powder was dried in an oven at 120 °C and subsequently passed through a sieve. The obtained powder was termed LaB<sub>6</sub>-ZAT.

To fabricate LaB<sub>6</sub>-ZAT ceramics, the LaB<sub>6</sub>-ZAT mixed powder was placed in a 30 mm diameter split graphite mold and then into a vacuum hot press sintering furnace. A temperature increase rate of 6 °C/min and an initial pressure of 7–8 MPa to 600 °C were first used. It was then heated to 1500–1900 °C in an argon atmosphere at a rate of 20 °C/min. Subsequently, it was maintained at this temperature for 1 h before being sintered through hot pressing at a uniaxial pressure of 30–60 MPa.

### 2.3. Characterization

The physical phase composition of the samples was analyzed using an X-ray diffractometer (XRD, D8 advanced, Bruker, Germany) which utilized Cu K<sub>α</sub> radiation with a 2θ test range of 20–80°. The samples' micro-morphology was characterized using a scanning electron microscope (SEM, S-4800, Hitachi, Tokyo, Japan). The median particle size of the powders was determined using a laser particle sizer (Mastersizer 2000, Malvern Ins, Malvern, UK).

The conductivity of the samples was assessed at a frequency of 60 kHz using an eddy current conductivity meter (Sigma 2008A, Tian Yan, Xiamen, China). The flexural strength was determined by a three-point bending test on an electronic universal testing machine (CMT4303, Meister Industrial Systems, Shenzhen, China). The size of the sample after machining was 20 × 2 × 2 mm. In the bending test, the span was selected as 16 mm, and the flexural strength ( $\sigma_b$ ) was calculated according to Formula (1). The samples' hardness was tested using a Vickers hardness tester (HMAS-010, Yan Run, Shanghai, China) on a grinding and polishing machine (MP-2B, Wei Yi, Laizhou, China) after polishing. The density of the ceramic was ascertained using the Archimedes method, with deionized water as the liquid medium, at room temperature. The theoretical density of LaB<sub>6</sub>-ZAT ceramics was computed based on the content of ZAT, with Formulas (2) and (3):

$$\sigma_b = \frac{3PL}{2bh^2} \quad (1)$$

$$\rho_{LaB_6-ZAT} = \frac{100 + n}{\frac{100}{\rho_{LaB_6}} + \frac{n}{\rho_{ZAT}}} \quad (2)$$

$$\rho_r = \frac{\rho}{\rho_{LaB_6-ZAT}} \times 100\% \quad (3)$$

In Formula (1),  $\sigma_b$  is the flexural strength,  $P$  is the maximum bending force,  $L$  is the span,  $b$  is the breadth, and  $h$  is the height.

In Formulas (2) and (3),  $\rho_{ZAT}$  is the theoretical density of the ZAT powder, which can be calculated from the mass ratio of the oxides;  $\rho_{LaB_6-ZAT}$  is the theoretical density of the LaB<sub>6</sub>-ZAT ceramic;  $n$  is the content of the ZAT powder;  $\rho_{LaB_6}$  is the theoretical density of the LaB<sub>6</sub> ceramic;  $\rho_r$  is the relative density of the LaB<sub>6</sub>-ZAT ceramic; and  $\rho$  is the volume density of the LaB<sub>6</sub>-ZAT ceramic.

## 3. Results

This section investigates the effects of the raw material particle size, ZAT content, temperature, and pressure on the densification, mechanical properties, and electrical properties of LaB<sub>6</sub> ceramics.

### 3.1. Effect of Particle Size

According to the theory of ceramic sintering, the powder particle size significantly impacts sintering. Consequently, raw powders with varying average particle sizes were selected for hot pressure sintering to compare the density of pure LaB<sub>6</sub> polycrystalline materials. The raw materials comprised commercial powders with average particle sizes of 20 μm and 10 μm, in addition to powders of various sizes that underwent ball milling. Figure 1 displays the variation in the cross-section morphology of ceramics prepared by hot-pressing LaB<sub>6</sub> powders with different particle sizes at 2000 °C and 40 MPa. Figure 2

shows the variation in the relative density, electrical conductivity, Vickers hardness, and flexural strength with particle size.

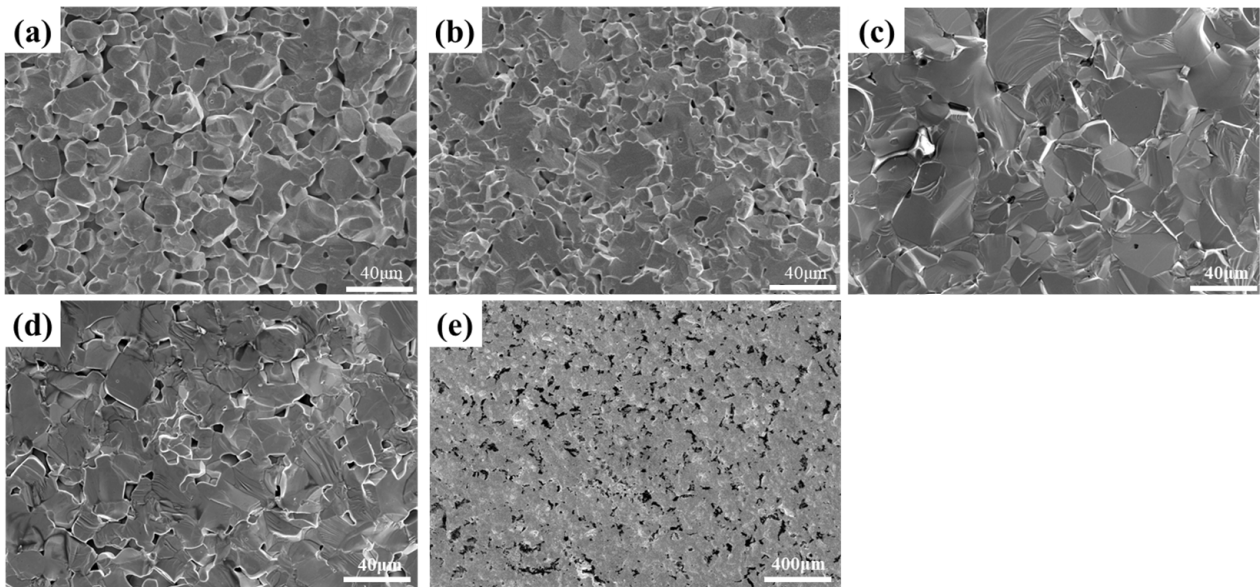


**Figure 1.** SEM images of LaB<sub>6</sub> ceramics at different average particle sizes: (a) 20 μm; (b) 10 μm; (c) 3.974 μm; (d) 2.826 μm; (e) 2.496 μm.

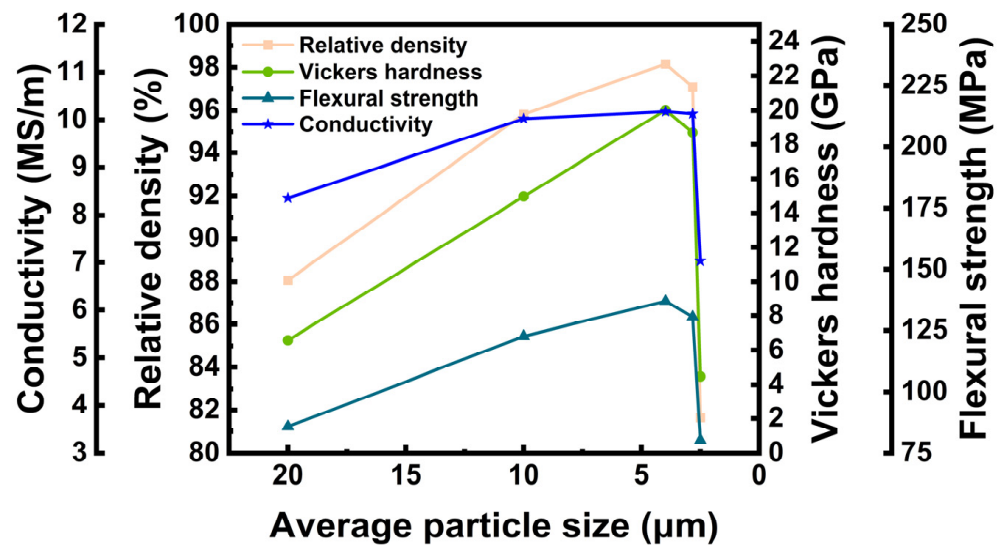


**Figure 2.** Relative density, conductivity, Vickers hardness, and flexural strength curve with average particle size.

Figure 1a–e showcases the cross-sectional morphology and pore distribution in LaB<sub>6</sub> ceramics prepared via hot pressing with raw materials of diverse particle sizes. With identical sintering conditions, a notable reduction in pores at the grain boundaries of LaB<sub>6</sub> ceramics occurs as the particle size of the raw materials diminishes. With increasing density, fractal-type cracks began to gradually emerge in the samples' cross-sectional morphology. This indicates the occurrence of transgranular fractures. Sections of ceramics, prepared by HPS of powders with an average grain size of 20 μm, demonstrate that the grains are only slightly connected to each other at the neck. When the average grain size is reduced to 10 μm, the cross-section shows tighter necking between grains. The pores consist of small closed pores within grains and open pores between grains. Figure 1c,d show fewer

pores at trident grain boundaries. However, for particle sizes as small as 2.496  $\mu\text{m}$ , the cross-section reveals numerous air holes between unsintered agglomerates. The changes in the number of pores in the sections are in line with the changes in relative density shown in Figure 2. For  $\text{LaB}_6$  ceramics, higher densities and fewer pores lead to better mechanical properties and electrical conductivity. As demonstrated in Figure 2, there is a positive correlation between Vickers hardness, flexural strength, and conductivity with density.  $\text{LaB}_6$  ceramics prepared with an average particle size of 3.974  $\mu\text{m}$  exhibited the highest relative density (98.16%), as well as the best Vickers hardness (20.02 GPa), flexural strength (136.95 MPa), and conductivity (10.18 MS/m). This performance is high compared to other  $\text{LaB}_6$  polycrystalline materials.

The change in density is also demonstrated by the variation in the number of pores at the same multiplicity on the polished surface of  $\text{LaB}_6$  ceramics, as depicted in Figure 3. It is evident that  $\text{LaB}_6$  ceramics prepared using HPS have larger grains, which is the reason why their mechanical properties are inferior to those of  $\text{LaB}_6$  nanocrystals.

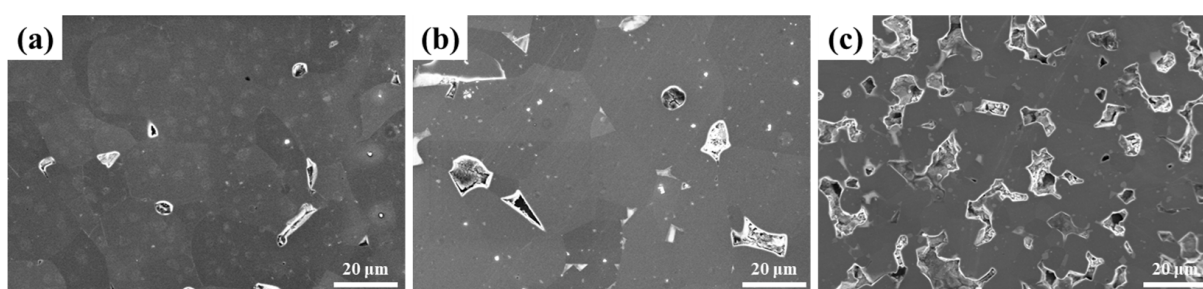


**Figure 3.** SEM images of polished surface of  $\text{LaB}_6$  ceramics at different average particle sizes: (a) 3.974  $\mu\text{m}$ ; (b) 2.826  $\mu\text{m}$ ; (c) 2.496  $\mu\text{m}$ .

High-energy ball milling effectively reduces the particle size of the raw material powder, enhancing its surface activity and promoting denser sintering. However, further reductions in particle size intensify the effect of powder agglomeration. Sintering particles within agglomerates demands a higher temperature than that required for sintering the agglomerates themselves. This leads to suboptimal powder densification during the sintering process.

### 3.2. Effect of ZAT Content

At present, the reported melting point of  $\text{LaB}_6$  is about 2700  $^{\circ}\text{C}$ , and its sintering temperature is generally in the temperature range of 1800–2100  $^{\circ}\text{C}$ . ZAT has the effect of reducing the sintering temperature, so 1700–1800  $^{\circ}\text{C}$  is chosen by us. The influence of ZAT contents, ranging from 3 to 8 wt.%, on the density of  $\text{LaB}_6$ -ZAT ceramics underwent investigation via HPS at temperatures of 1700–1800  $^{\circ}\text{C}$  and a pressure of 50 MPa. Figure 4 illustrates how the relative density of  $\text{LaB}_6$ -ZAT ceramics varies with differing ZAT contents at temperatures of 1700–1800  $^{\circ}\text{C}$  and a pressure of 50 MPa.

The data indicate that the relative density of  $\text{LaB}_6$ -ZAT ceramics increases and then slightly decreases with the increase in ZAT content. Nevertheless, the influence of content on density is modulated by the sintering temperature. For example, the graph demonstrates that the relative density of  $\text{LaB}_6$ -ZAT ceramics experiences significant variation with ZAT content at 1700  $^{\circ}\text{C}$ , while it stabilizes at 1800  $^{\circ}\text{C}$ . The reason for this is that the sintering temperature of  $\text{LaB}_6$  is approximately 1800  $^{\circ}\text{C}$ , and the sintering aid effect of ZAT is not significant. At a temperature of 1700  $^{\circ}\text{C}$ , the sintering aid has a significant effect on improving density. The maximum relative densities of 95.9% and 97.4% were achieved at sintering temperatures of 1700  $^{\circ}\text{C}$  and 1800  $^{\circ}\text{C}$ , respectively, with a ZAT content of 6 wt.%. Figure 5 shows the fracture surface of  $\text{LaB}_6$ -ZAT ceramics prepared with different ZAT contents at 1700  $^{\circ}\text{C}$ . As the content increases, the pores at the grain boundaries are eliminated and gradually reduced. Figure 6 shows the fracture surface of  $\text{LaB}_6$ -ZAT ceramics prepared with different ZAT contents at 1800  $^{\circ}\text{C}$ . Compared to the change in the

number of pores in the cross-section of the samples at 1700 °C, the change in the number of pores in the cross-section of the samples at 1800 °C is minimal, which is consistent with the trend of the change in relative density.

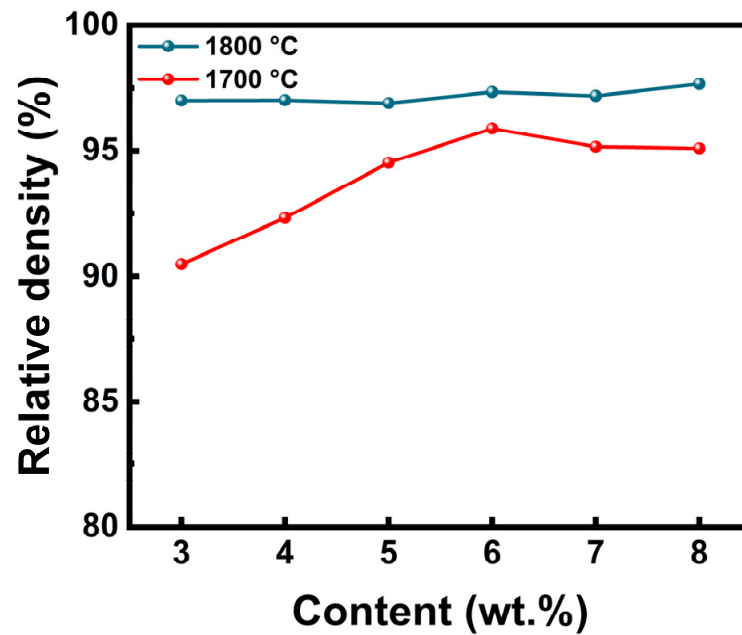


**Figure 4.** Relative density of LaB<sub>6</sub>-ZAT ceramics with different contents at 1700–1800 °C and 50 MPa (3 wt.%; 4 wt.%; 5 wt.%; 6 wt.%; 7 wt.%; 8 wt.%).

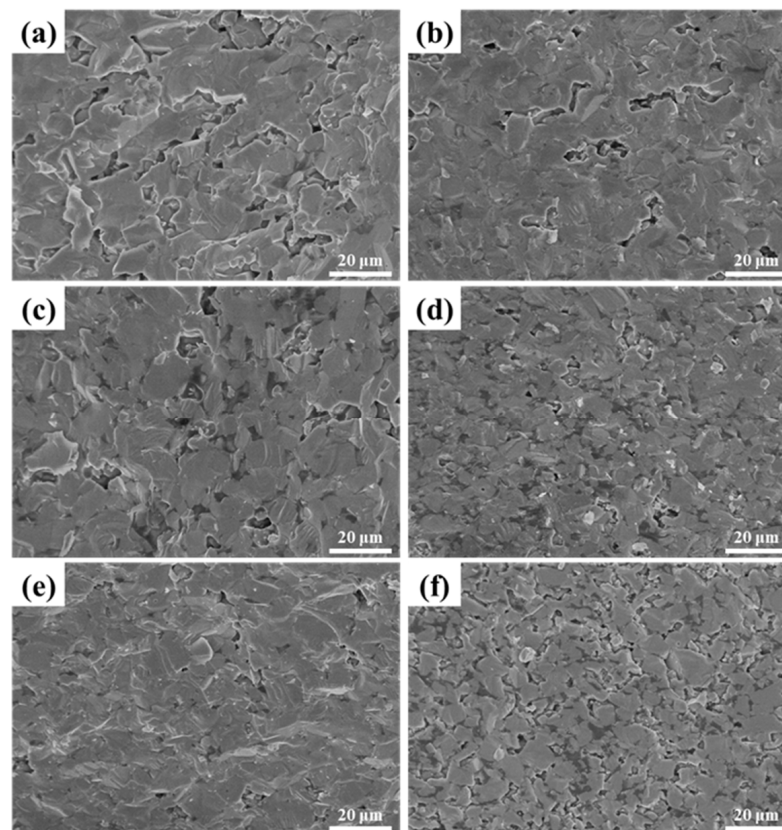


**Figure 5.** SEM images of LaB<sub>6</sub>-ZAT ceramics sintered with different contents at 1700 °C: (a) 3 wt.%; (b) 4 wt.%; (c) 5 wt.%; (d) 6 wt.%; (e) 7 wt.%; (f) 8 wt.%.

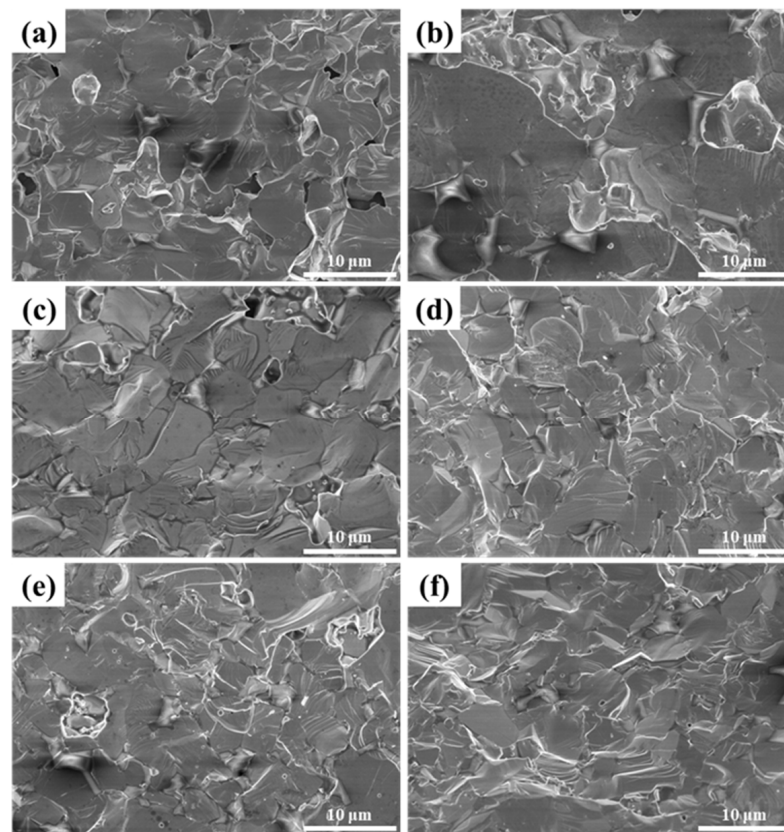


**Figure 6.** SEM images of  $\text{LaB}_6$ -ZAT ceramics sintered with different contents at  $1800\text{ }^\circ\text{C}$ : (a) 3 wt.%; (b) 4 wt.%; (c) 5 wt.%; (d) 6 wt.%; (e) 7 wt.%; (f) 8 wt.%.

Figure 7 shows the variation curve of the conductivity, flexural strength, and Vickers hardness of  $\text{LaB}_6$  ceramics with ZAT contents at different temperatures. At a sintering temperature of  $1700\text{ }^\circ\text{C}$ , the change in ZAT content has a greater impact on the ceramic properties compared to a sintering temperature of  $1800\text{ }^\circ\text{C}$ . The flexural strength and Vickers hardness of the ceramics at  $1700\text{ }^\circ\text{C}$  increased and then decreased with increasing ZAT content, as did the electrical conductivity. The mechanical and electrical properties of the ceramics prepared at  $1800\text{ }^\circ\text{C}$  show a weaker trend. Changes in the density of the ZAT content are closely related to these modifications, while the oxides have a direct impact on the mechanical and electrical properties of the ceramic, giving it less Vickers hardness and less conductivity.

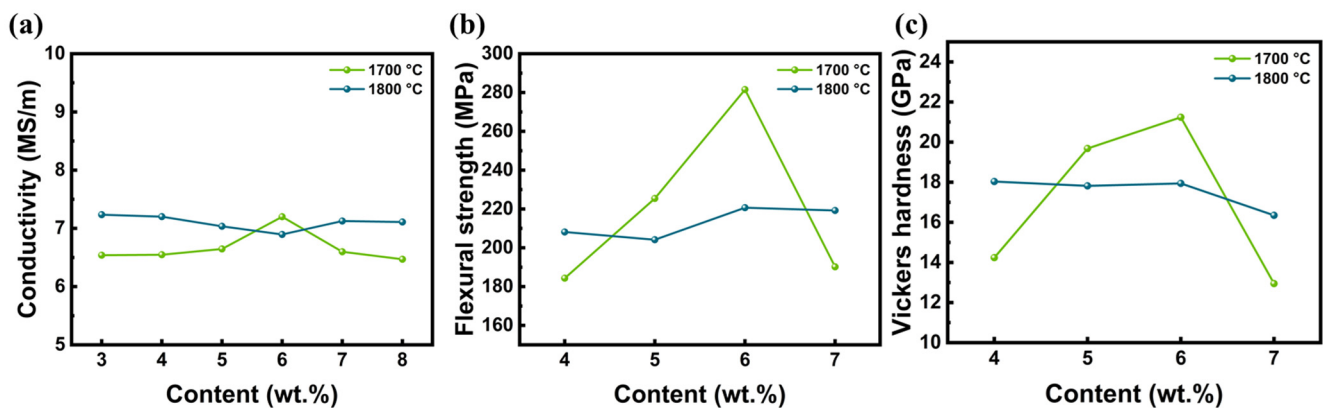


**Figure 7.** Properties of  $\text{LaB}_6$ -ZAT ceramics sintered with different contents at different temperatures: (a) conductivity; (b) flexural strength; (c) Vickers hardness.

In particular, the ceramic has the highest flexural strength of 281.5 MPa, the highest Vickers hardness of 21.2 GPa, and the highest conductivity of 7.2 MS/m at 6 wt.%. Based on this result, the ZAT content of the powders used in the subsequent experiments on the effect of temperature and pressure on properties was 6 wt.%.

### 3.3. Effect of Temperature

Based on the outcomes of preceding experiments, we determined optimal ball milling conditions to generate powder with an approximate average particle size of 4  $\mu\text{m}$  for hot pressure sintering and chose a ZAT addition of 6 wt.%. Prior research has indicated that the factors influencing sintering by hot pressing, ranked in descending order of importance, are sintering temperature, pressure, and holding time [24]. According to Tammann's Law, the temperature at which a solid's lattice undergoes plastic deformation and flow approximates to two-thirds of its melting point. The melting point of  $\text{LaB}_6$  is reported to be approximately 2700  $^\circ\text{C}$ , with the sintering temperature typically ranging between 1800 and 2100  $^\circ\text{C}$ .

#### 3.3.1. Low-Temperature Sintering

Depending on the experimental conditions and ZAT addition, a sintering temperature range of 1500 to 1900  $^\circ\text{C}$  was selected. This temperature range falls below that required for sintering pure  $\text{LaB}_6$  powder. Based on the outcomes of previous experiments, the holding time was established at 1 h, and the pressure was set between 30 and 60 MPa. [25].

Pure  $\text{LaB}_6$  powders and  $\text{LaB}_6$ -ZAT powders underwent hot pressure sintering at 50 MPa and different temperatures. Table 1 displays the results and relative densities. Clearly, at the same temperature,  $\text{LaB}_6$ -ZAT ceramics exhibit a higher relative density. Similarly, using  $\text{LaB}_6$ -ZAT powder allows for a reduction in sintering temperature to achieve the same density.

**Table 1.** Relative densities of ceramics.

Temperature ( $^\circ\text{C}$ )	$\text{LaB}_6$ Ceramics	$\text{LaB}_6$ -ZAT Ceramics
1500	78.17%	82.63%
1700	93.75%	95.91%
1900	97.08%	97.36%

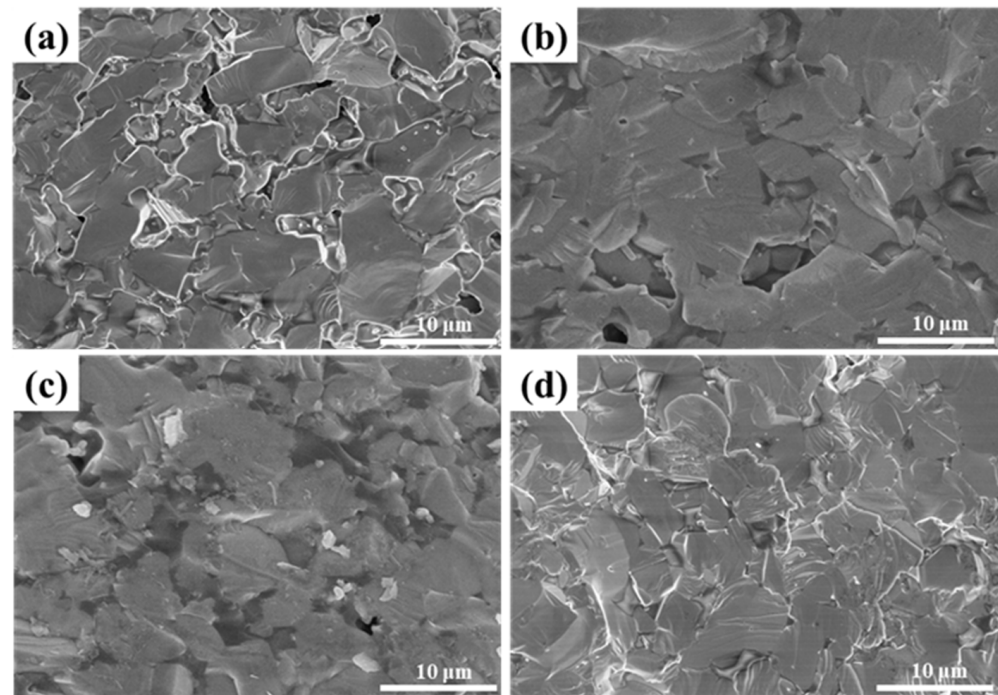
#### 3.3.2. Density and Properties of $\text{LaB}_6$ -ZAT Ceramics

Table 2 illustrates that the relative density and mechanical and electrical properties of  $\text{LaB}_6$ -ZAT ceramics varies with temperature at 50 MPa and 6 wt.% ZAT content. The data suggest that the relative density initially increases rapidly before decelerating as the sintering temperature rises. As the temperature increases (1500 to 1800  $^\circ\text{C}$ ), the activity of  $\text{LaB}_6$  powders increases so that more atoms overcome the diffusion barrier, and therefore, the diffusion coefficient increases. Moreover, with increasing temperatures, the degree of softening creep in the ZAT powders intensifies, positively affecting porosity reduction. Upon reaching temperatures of 1800 to 1900  $^\circ\text{C}$ , the relative density ceases to increase significantly. This can be attributed to the ideal sintering temperature for the raw material falling within this range.

**Table 2.** Relative density and properties of  $\text{LaB}_6$  ceramics at different sintering temperatures.

Temperature ( $^\circ\text{C}$ )	Relative Density (%)	Conductivity (MS/m)	Flexural Strength (MPa)	Vickers Hardness (GPa)
1500	82.63	4.42	214.85	6.33
1600	92.74	5.76	273.69	16.53
1700	95.91	7.20	281.54	21.24
1800	97.35	6.90	220.68	17.94
1900	97.36	-	-	-

Figure 8 displays the fracture surface of LaB<sub>6</sub>-ZAT ceramics prepared at various sintering temperatures. With increasing temperatures, pores at the grain boundaries are progressively eliminated and reduced. This observation indicates that the sintering temperature facilitates the densification process. Figure 9 displays the polished surface of LaB<sub>6</sub> ceramics at different temperatures. ZAT is located at the grain boundaries and can inhibit grain growth, resulting in improved mechanical properties. At a temperature of 1800 °C, the grain size of the ceramics increases, and the enhancement of ceramic flexural strength by ZAT at grain boundaries decreases.



**Figure 8.** SEM images of LaB<sub>6</sub> ceramics sintered at different temperatures: (a) 1500 °C; (b) 1600 °C; (c) 1700 °C; (d) 1800 °C.

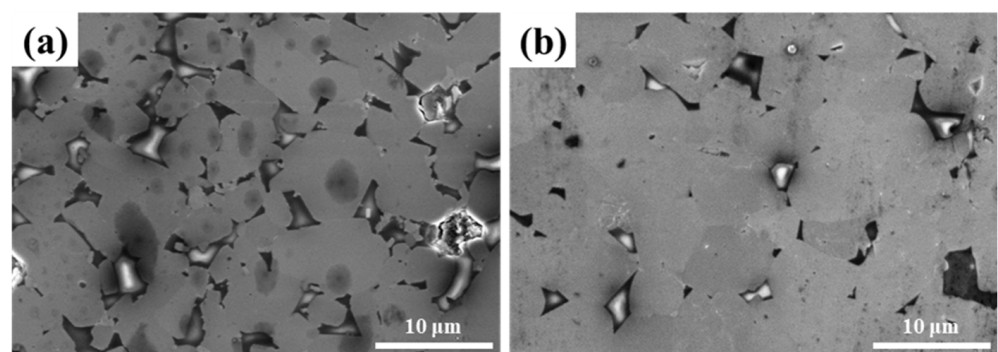


**Figure 9.** SEM images of polished surface of LaB<sub>6</sub> ceramics at different temperatures: (a) 1700 °C; (b) 1800 °C.

### 3.4. Effect of Sintering Pressure

Figure 10 illustrates how the relative density and properties of LaB<sub>6</sub>-ZAT ceramics vary with pressure at 1700 °C and 6 wt.% ZAT content. At 1700 °C, the relative density of ceramics tends to increase slightly with increasing pressure. This suggests that pressure has a minimal effect on ceramic sintering. Again, the mechanical and electrical properties of LaB<sub>6</sub>-ZAT ceramics are essentially flat with increasing pressure.

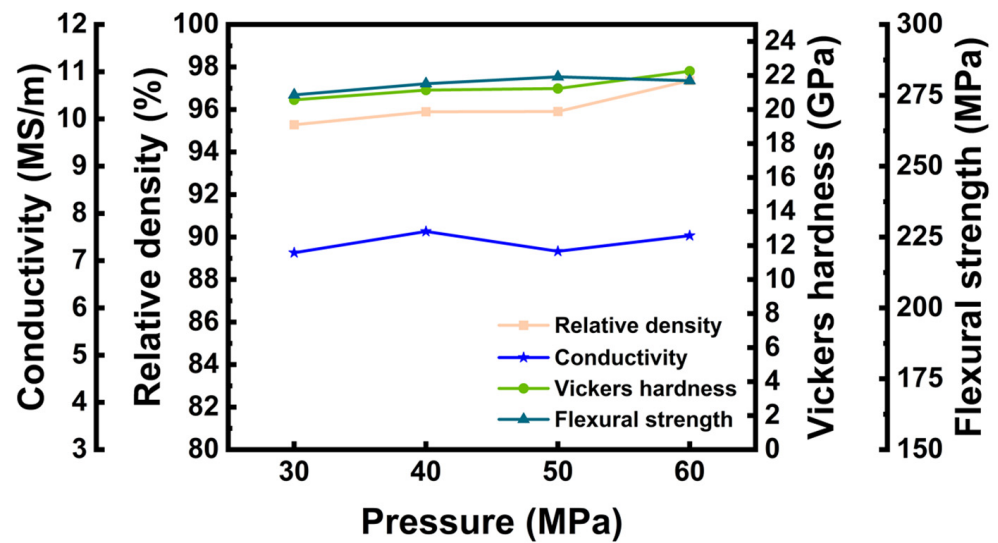


Figure 10. Relative density of LaB<sub>6</sub>-ZAT ceramics at different sintering pressures.

Figure 11 displays the fracture surface of LaB<sub>6</sub>-ZAT ceramics prepared at various pressures at 1700 °C. With increasing pressure, pores at the grain boundaries are progressively eliminated and reduced, although the changes are not significant, aligning with the relative density data. This is because increased pressure brings the particles closer together, resulting in diffusion over shorter distances. Furthermore, increasing pressure provides additional energy, thereby accelerating diffusion. Overall, pressure exerts minimal impact on the relative density of LaB<sub>6</sub> ceramics, significantly less than the impact of temperature.

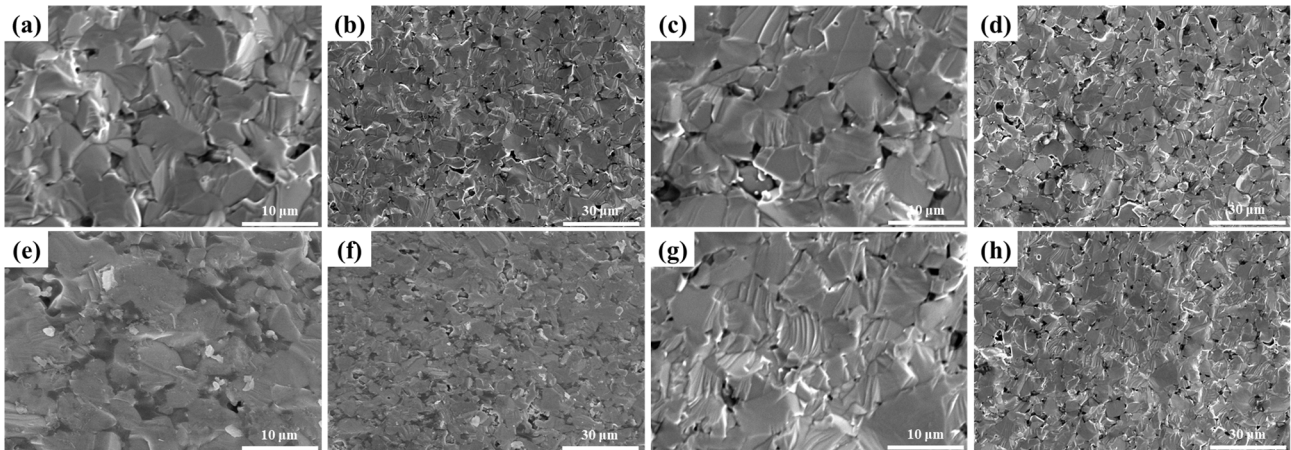


Figure 11. SEM images of LaB<sub>6</sub>-ZAT ceramics sintered at different sintering pressures: (a,b) 30 MPa; (c,d) 40 MPa; (e,f) 50 MPa; (g,h) 60 MPa.

#### 4. Discussion

The ceramics underwent X-ray diffraction tests to ascertain whether the addition of ZAT influenced the physical phase. Figure 12 illustrates the X-ray diffractograms of LaB<sub>6</sub>-ZAT ceramics produced through hot pressure sintering. We tested LaB<sub>6</sub>-ZAT ceramics prepared at various temperatures and with varying ZAT contents. The physical phases of these ceramics correspond well to the standard powder diffraction files of LaB<sub>6</sub>, with no heterogeneous phase generation. The LaB<sub>6</sub>-ZAT ceramics still have LaB<sub>6</sub> as the main crystalline phase. The results show that the addition of ZAT has no effect on the primary phase. There are two reasons for this phenomenon. Firstly, the content is too small to be detected. Secondly, the raw material has a low degree of crystallinity and is likely to form an amorphous phase when cooled.

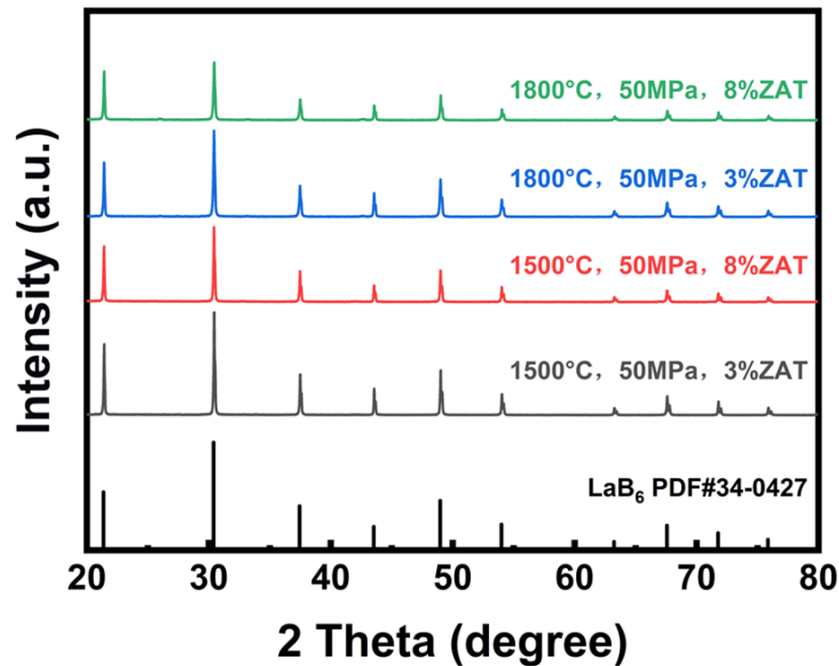


Figure 12. XRD patterns of  $\text{LaB}_6$ -ZAT ceramics prepared under different conditions.

Figure 13 presents the elemental mapping of the  $\text{LaB}_6$ -ZAT ceramic. The  $\text{LaB}_6$ -ZAT ceramic was prepared at 1700 °C and 50 MPa and the ZAT content was 6 wt.%, and it can be characterized as a representative sample. The distribution of ZAT at the grain boundaries is evident from the polished surface, indicated by the darker colored areas. The distributions of the B and La elements have almost identical shapes, with the La distribution showing greater abundance due to the heavier La element and the signals that can be collected at greater depths. The distribution of the elements (O, Zr, Al, Ti) is the same and complements the distribution of the B and La elements.

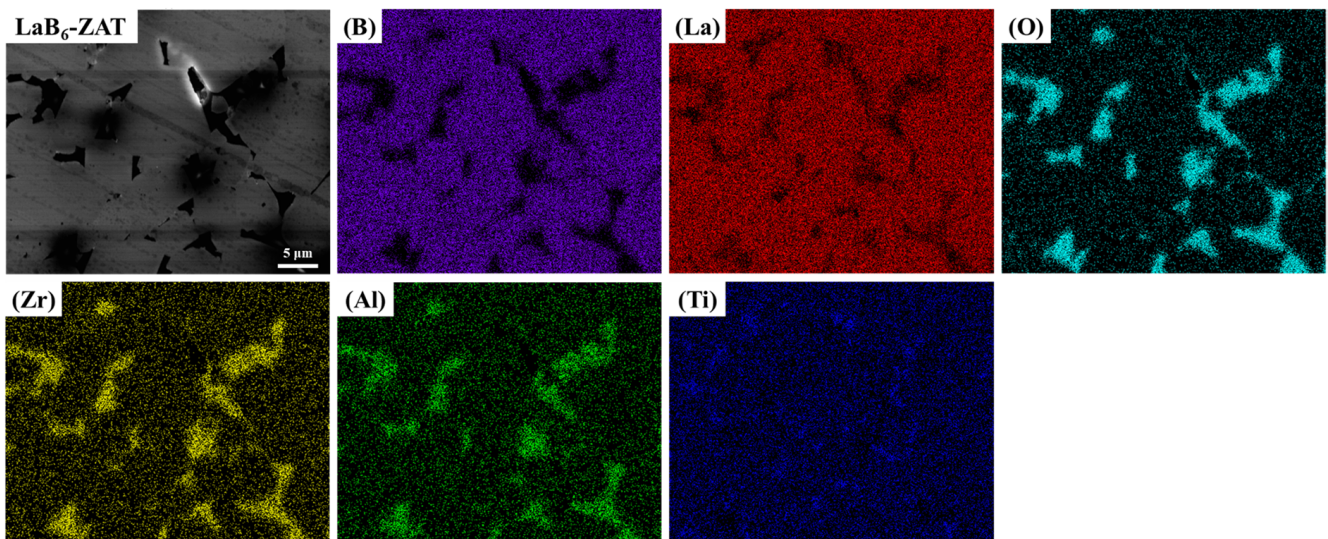
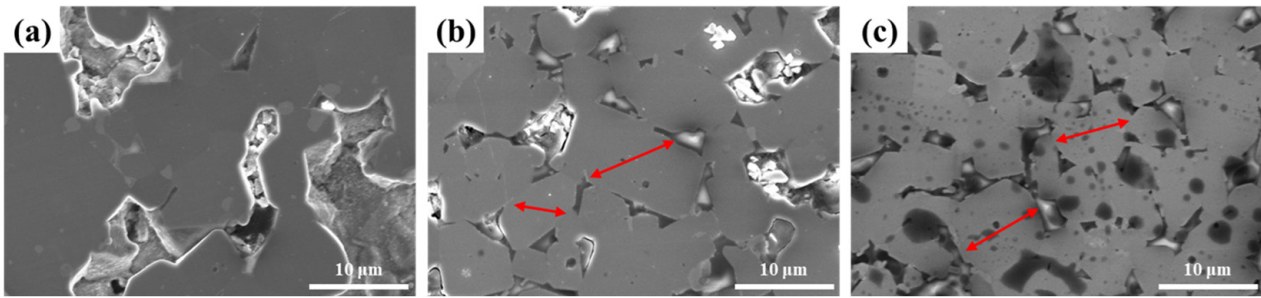


Figure 13. EDS patterns of polished surface of  $\text{LaB}_6$ -ZAT ceramic.

ZAT is located at the grain boundaries, inhibiting grain growth during sintering. The resulting  $\text{LaB}_6$ -ZAT ceramics have smaller grains, similar in size to the original powder grains. It is obvious from the red arrow in Figure 14 that the grain size of the ceramic after adding ZAT is smaller than that of pure  $\text{LaB}_6$  ceramics.



**Figure 14.** SEM images of polished surface of  $\text{LaB}_6$  and  $\text{LaB}_6$ -ZAT ceramics in different production conditions: (a) 2000 °C, 40 MPa, D50 = 2.493  $\mu\text{m}$ ; (b) 1700 °C, 40 MPa, 3 wt.% ZAT; (c) 1600 °C, 50 MPa, 8 wt.% ZAT.

During the three-point flexural experiment, the ZAT amorphous phase at the grain boundary before fracture absorbed some energy. Furthermore, the cross-sectional morphology shown in Figure 15 indicates the presence of crystal-penetrating fractures (red arrow), which results in a higher flexural strength of the ceramic compared to pure  $\text{LaB}_6$  ceramics.

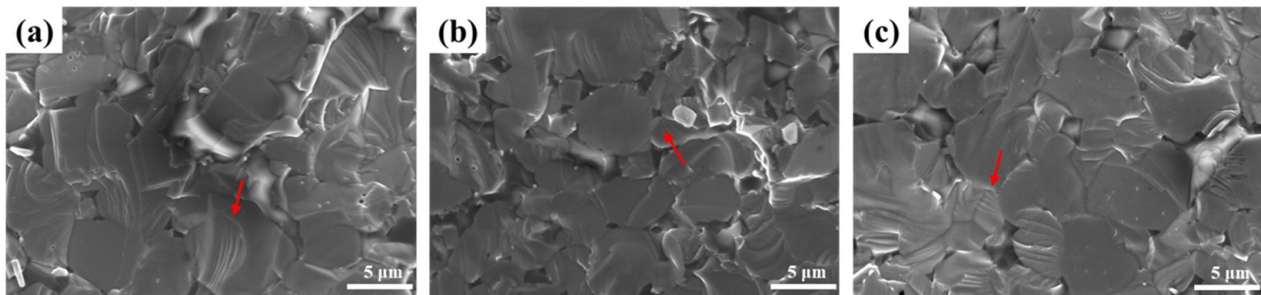


**Figure 15.** SEM images of  $\text{LaB}_6$ -ZAT ceramics prepared at different production conditions after bending fracture: (a) 1600 °C, 50 MPa, 6 wt.%; (b) 1700 °C, 50 MPa, 6 wt.%; (c) 1700 °C, 50 MPa, 8 wt.%.

Excellent electrical conductivity is a unique electrical property of  $\text{LaB}_6$  ceramics. The high electrical conductivity of  $\text{LaB}_6$  ceramics stems from the presence of free electrons within their crystal structure, making it comparable to metals. Excellent electrical conductivity is guaranteed, which allows the cathode material to be replenished with electrons for field emission applications.

Typically, oxides are insulators, possessing very low conductivity. The presence of ZAT at the grain boundaries may hinder electron transport in  $\text{LaB}_6$ -ZAT ceramics. However, as the density increases, the pores significantly reduce and the  $\text{LaB}_6$  grains come into direct contact with each other, despite the presence of ZAT at the grain boundaries. This results in an increase in the electron free range and conductivity. Of course, the conductivity of  $\text{LaB}_6$ -ZAT ceramics (4~7 MS/m) is lower than that of the pure  $\text{LaB}_6$  ceramics (7~10 MS/m) prepared by us. However, the conductivity of the  $\text{LaB}_6$ -ZAT ceramics falls within the range of conductivity observed for overall  $\text{LaB}_6$  polycrystalline or monocrystalline materials (3.3~10 MS/m). This is significant for practical applications.

## 5. Conclusions

This study reports pure  $\text{LaB}_6$  ceramics that were prepared using powders with an average particle size of 4  $\mu\text{m}$  under hot-pressing and sintering conditions at 2000 °C and 40 MPa for 1 h. The ceramics exhibited a relative density of 98.2%, a Vickers hardness of 20 GPa, a flexural strength of 136.9 MPa, and a conductivity of 10.2 MS/m.  $\text{LaB}_6$ -ZAT ceramics were prepared under hot-pressing and sintering conditions at 1700 °C and 50 MPa for 1 h. The first use of ZAT-composite  $\text{LaB}_6$  lowered the sintering temperature and, at the same time, resulted in a relative density of 97%. The dense  $\text{LaB}_6$ -ZAT ceram-

ics exhibited a flexural strength of 281.5 MPa and a Vickers hardness of 21.2 GPa, and the conductivity was measured at 7.2 MS/m. Our LaB<sub>6</sub>-ZAT ceramics, synthesized at 1700 °C, exhibit superior mechanical properties compared to pure LaB<sub>6</sub> ceramics hot-pressed at 2000 °C. Additionally, the electrical properties of our ceramics are highly promising for future applications.

**Author Contributions:** S.Y. completed the experiment and manuscript. W.M. completed the revision of the manuscript. R.B., J.H., J.L., J.G. and X.H. provided investigation and assistance for data analysis. H.Z. and N.Y. provided assistance for drawing and testing. All authors have read and agreed to the published version of the manuscript.

**Funding:** This research received no external funding.

**Institutional Review Board Statement:** Not applicable.

**Informed Consent Statement:** Not applicable.

**Data Availability Statement:** Data are contained within the article.

**Conflicts of Interest:** The authors declare no conflicts of interest.

## References

1. Lafferty, J.M. Boride cathodes. *J. Appl. Phys.* **1951**, *22*, 299–309. [[CrossRef](#)]
2. Broers, A. A new high resolution reflection scanning electron microscope. *Rev. Sci. Instrum.* **1969**, *40*, 1040–1045. [[CrossRef](#)] [[PubMed](#)]
3. Wang, Y.; Chou, K.C.; Zhang, G.H. Preparations of lanthanum hexaboride (LaB<sub>6</sub>) and cerium hexaboride (CeB<sub>6</sub>). *J. Am. Ceram. Soc.* **2022**, *105*, 1954–1966. [[CrossRef](#)]
4. Zhou, S.; Chen, K.; Cole, M.T.; Li, Z.; Chen, J.; Li, C.; Dai, Q. Ultrafast Field-Emission Electron Sources Based on Nanomaterials. *Adv. Mater.* **2019**, *31*, 1805845. [[CrossRef](#)] [[PubMed](#)]
5. Schmidt, P.; Joy, D. Low work function electron emitter hexaborides. *J. Vac. Sci. Technol.* **1978**, *15*, 1809–1810. [[CrossRef](#)]
6. Zhang, H.; Tang, J.; Zhang, Q.; Zhao, G.; Yang, G.; Zhang, J.; Zhou, O.; Qin, L.C. Field emission of electrons from single LaB<sub>6</sub> nanowires. *Adv. Mater.* **2006**, *18*, 87–91. [[CrossRef](#)]
7. Gan, H.; Peng, L.; Yang, X.; Tian, Y.; Xu, N.; Chen, J.; Liu, F.; Deng, S. A moderate synthesis route of 5.6 mA-current LaB<sub>6</sub> nanowire film with recoverable emission performance towards cold cathode electron source applications. *RSC Adv.* **2017**, *7*, 24848–24855. [[CrossRef](#)]
8. Liu, H.; Zhang, X.; Ning, S.; Xiao, Y.; Zhang, J. The electronic structure and work functions of single crystal LaB<sub>6</sub> typical crystal surfaces. *Vacuum* **2017**, *143*, 245–250. [[CrossRef](#)]
9. Tvaauri, I.; Silaev, I.; Zaalishvili, V.; Ashkhotov, O.; Sozaev, Z.; Magkoev, T. Reasons for the Low Work-Function Value of Lanthanum Hexaboride Used as an Efficient Electron Emitter. *Tech. Phys. Lett.* **2022**, *48*, 138–141. [[CrossRef](#)]
10. Zubeck, I.; Feigelson, R.; Huggins, R.; Pettit, P. The growth of lanthanum hexaboride single crystals by molten salt electrolysis. *J. Cryst. Growth* **1976**, *34*, 85–91. [[CrossRef](#)]
11. Tanaka, T.; Bannai, E.; Kawai, S.; Yamane, T. Growth of high purity LaB<sub>6</sub> single crystals by multi-float zone passage. *J. Cryst. Growth* **1975**, *30*, 193–197. [[CrossRef](#)]
12. Zhou, S.; Zhang, J.; Liu, D.; Lin, Z.; Huang, Q.; Bao, L.; Ma, R.; Wei, Y. Synthesis and properties of nanostructured dense LaB<sub>6</sub> cathodes by arc plasma and reactive spark plasma sintering. *Acta Mater.* **2010**, *58*, 4978–4985. [[CrossRef](#)]
13. Liu, H.; Zhang, X.; Xiao, Y.; Zhang, J. The electronic structures and work functions of (100) surface of typical binary and doped REB<sub>6</sub> single crystals. *Appl. Surf. Sci.* **2018**, *434*, 613–619. [[CrossRef](#)]
14. Zhou, S.; Zhang, J.; Liu, D.; Hu, Q.; Huang, Q. The effect of samarium doping on structure and enhanced thermionic emission properties of lanthanum hexaboride fabricated by spark plasma sintering. *Phys. Status Solidi (A)* **2014**, *211*, 555–564. [[CrossRef](#)]
15. Zhou, S.L.; Zhang, J.X.; Bao, L.H.; Yu, X.G.; Hu, Q.L.; Hu, D.Q. Enhanced thermionic emission properties in textured two-phase LaB<sub>6</sub>-BaB<sub>6</sub> system prepared by spark plasma sintering. *J. Alloys Compd.* **2014**, *611*, 130–134. [[CrossRef](#)]
16. Gao, R.L.; Min, G.H.; Yu, H.S.; Zheng, S.Q.; Lu, Q.L.; Han, H.D.; Wang, W.T. Fabrication and oxidation behavior of LaB<sub>6</sub>-ZrB<sub>2</sub> composites. *Ceram. Int.* **2005**, *31*, 15–19. [[CrossRef](#)]
17. Bogomol, I.; Nishimura, T.; Vasylykiv, O.; Sakka, Y.; Loboda, P. High-temperature strength of directionally reinforced LaB<sub>6</sub>-TiB<sub>2</sub> composite. *J. Alloys Compd.* **2010**, *505*, 130–134. [[CrossRef](#)]
18. Lu, H.H.; Huang, J.L. Effect Of Y<sub>2</sub>O<sub>3</sub> and Yb<sub>2</sub>O<sub>3</sub> on the microstructure and mechanical properties of silicon nitride. *Ceram. Int.* **2001**, *27*, 621–628. [[CrossRef](#)]
19. Zheng, Y.S.; Knowles, K.M.; Vieira, J.M.; Lopes, A.B.; Oliveira, F.J. Microstructure, toughness and flexural strength of self-reinforced silicon nitride ceramics doped with yttrium oxide and ytterbium oxide. *J. Microsc.* **2001**, *201*, 238–249. [[CrossRef](#)]
20. Matsunaga, C.; Zhou, Y.; Kusano, D.; Hyuga, H.; Hirao, K. Variation of porosity and pore size during post-sintering of reaction-bonded silicon nitride doped with Y<sub>2</sub>O<sub>3</sub> and MgO additives. *J. Ceram. Soc. Jpn.* **2020**, *128*, 75–79. [[CrossRef](#)]

21. Magnani, G.; Antolini, F.; Beaulardi, L.; Burrelli, E.; Coglitore, A.; Mingazzini, C. Sintering, high temperature strength and oxidation resistance of liquid-phase-pressureless-sintered SiC–AlN ceramics with addition of rare-earth ZrO<sub>2</sub>. *J. Eur. Ceram. Soc.* **2009**, *29*, 2411–2417. [[CrossRef](#)]
22. Rodríguez-Rojas, F.; Ortiz, A.L.; Borrero-López, O.; Guiberteau, F. Effect of the sintering additive content on the non-protective oxidation behaviour of pressureless liquid-phase-sintered  $\alpha$ -SiC in air. *J. Eur. Ceram. Soc.* **2010**, *30*, 1513–1518. [[CrossRef](#)]
23. Colkesen, P.; Kaplan, G.; Yoon, D.-H. Densification and high-temperature oxidation behavior of SiC sintered with multicomponent rare-earth additives. *Ceram. Int.* **2023**, *49*, 31163–31174. [[CrossRef](#)]
24. Yu, Y. Preparation and Doping Modification of LaB<sub>6</sub> Polycrystalline Cathode Materials. Ph.D. Thesis, National University of Defense Technology, Changsha, China, 2018.
25. Ba, R.; Ma, W.; Hong, J.; He, X.; Li, J.; Yang, S. Valence transition of cerium during the synthesis of powders and densification of CeB<sub>6</sub> polycrystalline. *J. Mater. Sci. Mater. Electron.* **2022**, *33*, 14097–14107. [[CrossRef](#)]

**Disclaimer/Publisher’s Note:** The statements, opinions and data contained in all publications are solely those of the individual author(s) and contributor(s) and not of MDPI and/or the editor(s). MDPI and/or the editor(s) disclaim responsibility for any injury to people or property resulting from any ideas, methods, instructions or products referred to in the content.